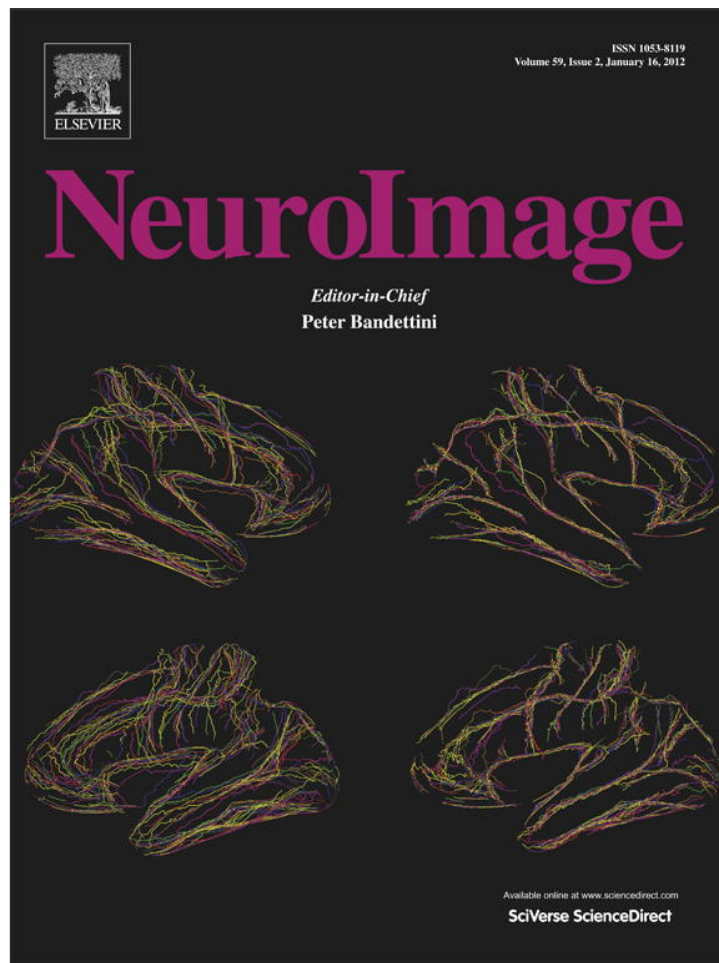


Provided for non-commercial research and education use.  
Not for reproduction, distribution or commercial use.



(This is a sample cover image for this issue. The actual cover is not yet available at this time.)

This article appeared in a journal published by Elsevier. The attached copy is furnished to the author for internal non-commercial research and education use, including for instruction at the authors institution and sharing with colleagues.

Other uses, including reproduction and distribution, or selling or licensing copies, or posting to personal, institutional or third party websites are prohibited.

In most cases authors are permitted to post their version of the article (e.g. in Word or Tex form) to their personal website or institutional repository. Authors requiring further information regarding Elsevier's archiving and manuscript policies are encouraged to visit:

<http://www.elsevier.com/copyright>



Contents lists available at SciVerse ScienceDirect

NeuroImage

journal homepage: [www.elsevier.com/locate/ynimg](http://www.elsevier.com/locate/ynimg)

Cognitive: Executive Function

## Dissociable large-scale networks anchored in the right anterior insula subserve affective experience and attention

 Alexandra Touroutoglou<sup>a,b</sup>, Mark Hollenbeck<sup>a,b,c</sup>, Bradford C. Dickerson<sup>a,b,c,1</sup>, Lisa Feldman Barrett<sup>a,b,d,1,\*</sup>
<sup>a</sup> Athinoula A. Martinos Center for Biomedical Imaging, Massachusetts General Hospital and Harvard Medical School, Charlestown, Massachusetts, USA

<sup>b</sup> Psychiatric Neuroimaging Research Program, Massachusetts General Hospital and Harvard Medical School, Charlestown, Massachusetts, USA

<sup>c</sup> Department of Neurology, Massachusetts General Hospital and Harvard Medical School, Boston, Massachusetts, USA

<sup>d</sup> Department of Psychology, Northeastern University, Boston, Massachusetts, USA

### ARTICLE INFO

#### Article history:

Received 12 November 2011

Revised 25 January 2012

Accepted 4 February 2012

Available online 13 February 2012

#### Keywords:

Dorsal anterior insula

Ventral anterior insula

Intrinsic functional connectivity

Individual differences

Attention

Processing speed

Affective experience

### ABSTRACT

Meta-analytic summaries of neuroimaging studies point to at least two major functional-anatomic subdivisions within the anterior insula that contribute to the detection and processing of salient information: a dorsal region that is routinely active during attention tasks and a ventral region that is routinely active during affective experience. In two independent samples of cognitively normal human adults, we used intrinsic functional connectivity magnetic resonance imaging to demonstrate that the right dorsal and right ventral anterior insula are nodes in separable large-scale functional networks. Furthermore, stronger intrinsic connectivity within the right dorsal anterior insula network was associated with better performance on a task involving attention and processing speed whereas stronger connectivity within the right ventral anterior insula network was associated with more intense affective experience. These results support the hypothesis that the identification and manipulation of salient information is subserved by at least two brain networks anchored in the right anterior insula that exhibit distinct large-scale topography and dissociable behavioral correlates.

© 2012 Elsevier Inc. All rights reserved.

### Introduction

The insula is a major cortical region in the human brain buried in the depth of the Sylvian fissure, enclosed by frontoparietal opercular cortex and superior temporal cortex. Activation foci in the anterior insula (AI) are among the most commonly found in functional neuroimaging experiments across both affective and cognitive domains (Nelson et al., 2010). For example, the AI shows increased activation in studies of affect and emotion (Bartels and Zeki, 2004; Damasio et al., 2000; Heining et al., 2003; Jabbi et al., 2008; Kober et al., 2008; Lindquist et al., in press; Phan et al., 2004; Small et al., 2001) as well as visceral sensations that many view as the physiological basis of “feelings” (Craig, 2009, 2011; Critchley, 2009; Critchley et al., 2005) such as temperature sensation (Hua le et al., 2005), awareness of heartbeat (Critchley et al., 2004), dyspnea (Banzett et al., 2000), and pain (Brooks et al., 2005; Craig et al., 2000). Additionally, the AI

is involved in a variety of cognitive functions, such as orienting of attention (Corbetta and Shulman, 2002), cognitive control (Cole and Schneider, 2007), performance monitoring (Dosenbach et al., 2006), and the detection of salient information (Seeley et al., 2007).

Tract tracing studies in non-human primates show that the AI has reciprocal connections to many cortical and subcortical structures that are also implicated in affect and attention (Augustine, 1996). The dysgranular dorsal anterior insula (dAI) is reciprocally connected with multiple isocortical regions in prefrontal cortex, precentral operculum, parietal, and temporal cortex. The agranular ventral anterior insula (vAI) is reciprocally connected with multiple limbic and paralimbic structures including pregenual anterior cingulate cortex (pgACC), entorhinal and periamygdaloid cortex, temporal pole, and lateral orbitofrontal cortex (OFC) (Mesulam and Mufson, 1982a,b; Mufson and Mesulam, 1982). Thus, the AI serves as an integrative paralimbic hub between isocortical and limbic cortical zones. Although the connective topography of the AI in the monkey has been known for 30 years, methods have only recently been developed to map human brain anatomic connectivity. Using probabilistic tractography and diffusion tensor imaging, Cerliani et al. (2011) examined the insula connectivity in humans and demonstrated that a region within vAI has strong anatomic connections with subcortical regions such as amygdala, hippocampus, and entorhinal cortex. Unlike the vAI, a region within dAI had strong anatomic connections with the inferior frontal gyrus (Cerliani et al., 2011). Consistent with

**Abbreviations:** dAI, dorsal anterior insula; vAI, ventral anterior insula; rs-fc-MRI, resting state functional connectivity magnetic resonance imaging; pgACC, pregenual anterior cingulate cortex; ICC, intraclass correlation coefficients; FPA, frontopolar area; MFG, middle frontal gyrus; SMG, supramarginal gyrus; OFC, orbitofrontal cortex.

\* Corresponding author at: Department of Psychology, 253 Nightingale Hall, Northeastern University, Boston, MA 02115, USA. Tel.: +1 617 373 2044; fax: +1 617 373 8714.

E-mail address: [lbarrett@neu.edu](mailto:lbarrett@neu.edu) (L. Feldman Barrett).

<sup>1</sup> These authors contributed equally to the research.

the findings on the anatomic connectivity, two recent studies mapping the intrinsic connectivity within the human AI have demonstrated variation in connectivity along the dorsal/ventral axis (Deen et al., 2011; Nelson et al., 2010), specifically showing that dAI is connected with dorsal anterior cingulate cortex (dACC) and other frontal and parietal regions whereas the vAI is connected with pgACC and superior temporal cortex.

Meta-analytic studies of the neuroimaging literature also point to a functional differentiation of dAI and vAI (Kurth et al., 2010; Mutschler et al., 2009; Small, 2010; Wager and Barrett, 2004). The dAI appears to be relatively more engaged during attention and executive function tasks, whereas the vAI appears to be relatively more engaged during affective or emotional tasks (Kurth et al., 2010; Wager and Barrett, 2004). To our knowledge, this behavioral dissociation between dAI and vAI has not yet been demonstrated in a single experiment.

In this study, we used resting state functional connectivity magnetic resonance imaging (rs-fcMRI) in healthy adults to build upon this prior work. rs-fcMRI reflects the temporal correlations between low frequency Bold Oxygen Level-Dependent (BOLD) signal fluctuations of brain areas and as such provides a basis for understanding the large-scale anatomic organization of brain networks (Buckner, 2010; Deco et al., 2011; Fox and Raichle, 2007; Vincent et al., 2007). rs-fcMRI provides unique information about the neural circuit of interest that goes beyond anatomy and task-driven functional connectivity. The topography of intrinsic connectivity networks revealed by rs-fcMRI is constrained by anatomy and is fairly stable across individuals and resting state conditions (Damoiseaux et al., 2006; Van Dijk et al., 2010). Yet the strength of intrinsic connectivity can be modulated by previous experience (Stevens et al., 2010; Tambini et al., 2010) and provides measures that relate to individual differences in behavior (Di Martino et al., 2009; Fox et al., 2007; Hampson et al., 2006; Lewis et al., 2009; Seeley et al., 2007; Wang et al., 2010a; Wang et al., 2010b). Here, in two separate samples, we first replicated and expanded the finding that distinct dAI and vAI regions are nodes in separable large-scale functional-anatomic networks, with preferential connections between the dAI and frontoparietal regions implicated in attention and between the vAI and regions implicated in affect such as pgACC, OFC, and amygdala. Second, we hypothesized that stronger connectivity within the dAI network would be specifically associated with individual differences in attention whereas stronger connectivity within the vAI network would be specifically associated with individual differences in the intensity of affective experience.

## Materials and Methods

### Participants

Sample 1 consisted of 89 young adults (44 men) ranging in age from 18 to 33, with a mean age of 22.4 years ( $SD=3.34$ ) [resting state data from these participants have been previously published in Yeo et al. (2011)]. Sample 2 consisted of 31 young adults ranging in age from 19 to 32, with a mean of age = 24.2 years ( $SD=2.89$ ; 11 men) [subjective reports of arousal from these participants have been previously published as part of a larger project on age-related differences in affect and novelty processing (Moriguchi et al., 2011; Weierich et al., 2010)]. Of the original 31 participants with resting state BOLD data, 30 (11 men) also reported on their subjective arousal when viewing evocative images [i.e., ratings of subjective affective arousal made on-line as people viewed affectively potent images from the International Affective Picture Set (IAPS) (Lang et al., 1997)] and 25 (11 men) also completed the Trail Making Test (Reitan, 1958). All participants in both samples were right-handed, native English speakers and had normal or corrected-to-normal vision. No participant reported a history of neurological or psychiatric disorders.

### fMRI data acquisition and preprocessing procedures

Data were collected from a 3 Tesla Tim Trio System (Siemens Medical Systems, Erlangen, Germany), using a 12-channel phased-array head coil. Structural data were acquired using a 3D T1-weighted magnetization-prepared gradient-echo image (MPRAGE) [Sample 1: repetition time (TR)=2200 ms; echo time (TE)=1.54 ms; flip angle (FA)=7°, 1.2 mm isotropic voxels; Sample 2: TR=2530 ms; TE=3.5 ms; FA=7°, 1.0 mm isotropic voxels]. Whole-brain fMRI data were acquired with echo-planar sequence [Sample 1: TR=3000 ms; TE=30 ms; FA=85°; 3.0 mm isotropic voxels, 47 slices; Sample 2: TR=2000 ms; TE=30 ms; FA=90°; 3.1×3.1×5.0 mm voxels, 33 slices). Sample 1 involved two ( $n=87$ ) or four ( $n=2$ ) runs of 124 time points and Sample 2 involved one ( $n=6$ ) or two ( $n=25$ ) runs of 128 time points. For Sample 2 with two runs, the affective experience task was administered before the second run. During the resting-state fMRI runs, participants in both samples were instructed to keep their eyes open. Head motion was minimized using head restraints, including a pillow and foam padding. Noise was attenuated with ear plugs.

Preprocessing of the fMRI data involved a series of previously established rs-fcMRI procedures (Biswal et al., 1995; Van Dijk et al., 2010; Vincent et al., 2007) including: (1) removal of the four volumes to allow for T1 equilibration effects, (2) slice timing correction (SPM2, Wellcome Department of Cognitive Neurology, London, United Kingdom), and (3) head motion correction (FMRIB, Oxford, UK). Data were normalized to the Montreal Neurological Institute (MNI) atlas space (SPM2, Wellcome Department of Cognitive Neurology, London, United Kingdom) and re-sampled to 2mm cubic voxels. A low-pass temporal filter removed frequencies higher than 0.08Hz. Data were spatially smoothed using a 6 mm full-width half-maximum Gaussian filter. Sources of spurious variance and their temporal derivatives were removed through linear regression including: (1) six parameters obtained by rigid-body correction of head motion correction, (2) the signal averaged over the whole brain, (3) the signal averaged over the ventricles, and (4) the signal averaged over the deep cerebral white matter.

### Behavioral data acquisition

#### Affective experience

One hundred thirty-two full-color images were selected from the International Affective Picture System (Lang et al., 1997) for each of six combinations of arousal and valence (i.e., high arousal negative, high arousal positive, mid arousal negative, mid arousal positive, mid arousal neutral, and low arousal neutral images).

The task was run using E-Prime experimental software (Psychology Software Tools, Pittsburgh, PA) on a PC, from which images were projected onto a screen in the magnet bore. Participants viewed images via a mirror mounted on the head coil. The task consisted of five event-related fMRI runs. The first run was a familiarization run. Participants were familiarized to two images in each stimulus category (12 pictures total). The 12 IAPS images were each shown 10 times. Throughout four test runs, participants viewed each familiarized image a total of 10 times and each of the 120 novel images only once. Each run was 340 sec in length and each image was presented for 3.5 sec, with a stimulus onset asynchrony that varied from 4 to 16 sec.

Participants used a 3-button response to rate how aroused (1 = low, 2 = mid, 3 = high) each image made them feel. The subjective arousal ratings were then averaged to create composite measures of affective experience for use in behavioral correlation analyses. Subjective arousal ratings to high arousal novel and high arousal familiarized negative images were averaged to create a composite measure of negative affective experience. Subjective arousal ratings to high

arousal positive images were averaged to create a composite measure of positive affective experience.

#### Attention

Attention was measured with the Trail Making Test administered before the scans (Reitan, 1958; Strauss et al., 2006). The Trail Making Test is commonly used for neuropsychological assessment of attention, processing speed, and set-switching (Strauss et al., 2006), processes that consistently activate areas within the dAI (Dosenbach et al., 2007; Mutschler et al., 2009; Nelson et al., 2010; Wager and Barrett, 2004). For each participant, the Trail Making Test A (or Trail Making Test B) score reflected the time in seconds taken to complete the part A (or B) of the test. Trail Making Test A time is thought to require processing speed, motor speed, and visual search, whereas Trail Making Test B additionally requires set-switching (Strauss et al., 2006).

#### Functional connectivity analysis

##### Analysis of the topography and strength of insular subregion connectivity

To explore the topography of functional connectivity of the AI, we used whole brain seed-based rs-fMRI analysis in Sample 1. Two spherical regions of interest (ROIs) (4-mm radius) were used as seed regions, right dAI (right dAI coordinates: +36, 21, 1, MNI) and right vAI (right vAI coordinates: +28, 17, -15). The coordinates of the two AI seeds were determined from a meta-analysis of AI activations (Kurth et al., 2010), showing that the dAI is preferentially activated in working memory tasks, whereas the vAI is preferentially activated in emotion tasks. To examine the functional connectivity of the right dAI<sub>seed</sub> and right vAI<sub>seed</sub>, we computed Pearson's product moment correlations,  $r$ , between the mean signal time course of the AI<sub>seeds</sub> and the time course of all voxels across the brain. The resulting correlation maps were converted to  $z$ -values, using Fisher's  $r$ -to- $z$  transformation and were averaged across subjects. The locations of the right dAI and right vAI correlation peaks were determined with visual inspection of each of the two correlation maps independently, using the FSL view toolbox (<http://www.fmrib.ox.ac.uk/fsl>). The minimum threshold was set to  $z(r) = 0.2$  (Van Dijk et al., 2010). Using FSL's Harvard-Oxford cortical and subcortical structural probabilistic atlases (<http://www.fmrib.ox.ac.uk/fsl/data/atlas-descriptions.html>), a voxel with the highest  $z(r)$  value was located within each anatomical structure.

To quantify the strength of functional connectivity between the seed and target regions, we created spherical ROIs (4-mm radius) around each correlation peak. Fisher's  $r$ -to- $z$  correlation coefficients were then calculated between each pair of seed-to-target ROIs (dAI<sub>seed</sub>-to-dAI<sub>targets</sub> and vAI<sub>seed</sub>-to-vAI<sub>targets</sub>). Next, for each network, we calculated three summary connectivity measures for use in reliability and behavioral analyses. To define metrics of connectivity strength for the dAI network, we computed: a) a dAI-to-dACC/paracingulate connectivity measure, i.e., a single pairwise connectivity measure of  $z(r)$  values between the dAI<sub>seed</sub> and its target region in dACC/paracingulate cortex that represents a major node of the "cingulo-operculum control" network (Dosenbach et al., 2006); b) a dAI-to-frontoparietal ROIs connectivity measure, i.e., a composite pairwise connectivity measure of  $z(r)$  values between the dAI<sub>seed</sub> and its target sites in or around other major regions of the "frontoparietal control" network as delineated by Vincent et al. (2008), including dACC/paracingulate, supramarginal gyrus (SMG), and middle frontal gyrus (MFG); and c) a dAI<sub>seed</sub>-to-dAI<sub>target</sub> ROIs connectivity measure, i.e., a connectivity measure of  $z(r)$  values between the dAI<sub>seed</sub> and all of its target regions. Correspondingly, to define a metric of connectivity strength for the vAI network, we calculated: a) a vAI-to-pgACC connectivity measure, i.e., a single pairwise connectivity measure of  $z(r)$  values between the vAI<sub>seed</sub> and its target region in pgACC, two major components of the "salience network" described by Seeley et al. (2007),

termed frontoinsula and dACC in that manuscript; b) a vAI-to-fronto-lingual-striatal ROIs connectivity measure, i.e., a composite pairwise connectivity measure of  $z(r)$  values between the vAI<sub>seed</sub> region and target sites in or around other major regions of the "salience network" (Seeley et al., 2007), including frontopolar area (FPA), pgACC, and ventral striatum; and c) a vAI<sub>seed</sub>-to-vAI<sub>targets</sub> connectivity measure, i.e., a connectivity measure of  $z(r)$  values between the vAI<sub>seed</sub> and all of its target regions.

To directly compare the spatial topography of the dAI and vAI networks, we binarized the group-level dAI and vAI connectivity maps and computed their spatial disjunction and conjunction. We also visualized these maps in FreeSurfer on the *fsaverage* cortical surface template (<http://surfer.nmr.mgh.harvard.edu>).

#### Reliability of distinct large-scale networks anchored in the AI

To test the reliability of the spatial topography of the two AI networks, we used the ROIs defined in Sample 1 and tested whether the dAI and vAI maps replicate in an independent sample (Sample 2). In all other respects, the analysis procedure was identical to that used in Sample 1. To assess the reliability of the strength of connectivity of the two networks, we computed intraclass correlation coefficients (ICC) (two way random effects with absolute agreement) between the averaged  $z(r)$  values of each seed-to-target ROI pair (dAI<sub>seed</sub>-to-dAI<sub>targets</sub> and vAI<sub>seed</sub>-to-vAI<sub>targets</sub>) in Sample 1 and the averaged  $z(r)$  values of each seed-to-target ROI pair (dAI<sub>seed</sub>-to-dAI<sub>targets</sub> and vAI<sub>seed</sub>-to-vAI<sub>targets</sub>) in Sample 2, using PASW Statistics 18, Release Version 18.0.0 (SPSS, Inc., 2009, Chicago, IL, [www.spss.com](http://www.spss.com)).

#### Behavioral correlation analyses

We examined in Sample 2 whether the connectivity strength of the right dAI and right vAI networks predicted individual differences in attention and affective experience, respectively. To test the convergent validity predictions for the right dAI network, we used the three summary connectivity measures for the right dAI network as independent variables and examined their ability to predict variation in two attention dependent variables (Trail Making Test A time and Trail Making Test B time). To test the convergent validity predictions for the right vAI network, we used the three summary right vAI network connectivity measures as independent variables and examined their ability to predict variation in the two affective dependent variables (the intensity of subjective affective experiences when viewing positive or negative pictures). Correspondingly, we evaluated the discriminant validity for each network by examining how well right dAI connectivity predicted the intensity of affective experience and how well right vAI connectivity predicted Trail Making Test performance.

## Results

### Distinct large-scale networks anchored in the right dAI and right vAI

Similar to prior work (Deen et al., 2011; Nelson et al., 2010), we found that dAI and vAI were nodes in separable large-scale functional-anatomic networks. Sample 1 revealed two large-scale AI networks of distinct spatial topography (Fig. 1). Intrinsic BOLD signal fluctuations within the right dAI<sub>seed</sub> were preferentially correlated with signal fluctuations in frontal, parietal, and dACC/paracingulate regions bilaterally. Frontal targets included FPA, MFG, inferior frontal gyrus, supplementary motor area, and precentral gyrus. Bilateral parietal regions included parietal operculum, superior parietal lobule, and anterior and posterior parts of SMG. Medially, intrinsic BOLD signal fluctuations within the right dAI<sub>seed</sub> were correlated with signal fluctuations in dACC/mid cingulate and adjacent paracingulate cortex. Furthermore, within the insula itself, right dAI signal correlated with signal fluctuations in bilateral mid and posterior insular regions

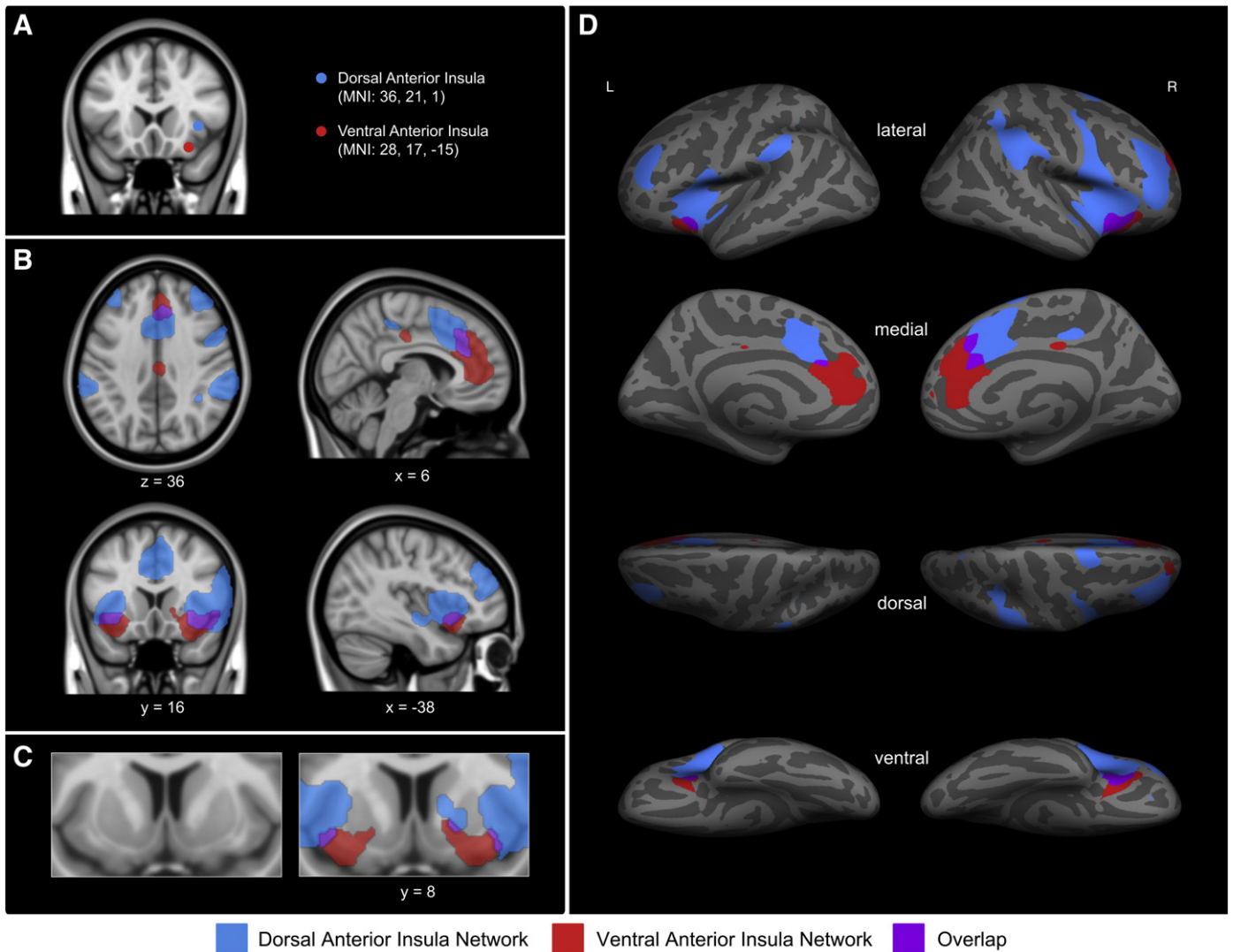


**Fig. 1.** In the exploratory analyses performed using Sample 1, the right dorsal anterior insula seed ( $dAI_{seed}$ , blue) and right ventral anterior insula seed ( $vAI_{seed}$ , red) (A) have distinct patterns of intrinsic functional connectivity at  $z(r) > 0.2$ ; (B and C) regions that preferentially correlate with the right  $dAI_{seed}$  are shown in blue, regions that preferentially correlate with the right  $vAI_{seed}$  are shown in red, and regions that correlate with both seeds are shown in purple. For display purposes, the binarized correlation maps,  $z(r) > 0.2$ , were upsampled (interpolated) to 1mm and overlaid on the 1mm MNI152 T1-standard template image in FSL and on (D) the inflated cortical surfaces of the left and right hemisphere (the *fsaverage* template in FreeSurfer). (For interpretation of the references to color in this figure legend, the reader is referred to the web version of this article.)

as well as adjacent frontal operculum and central operculum. Other right  $dAI_{targets}$  were found in lateral occipital cortex, superior temporal pole, and dorsal putamen.

As predicted, the intrinsic BOLD signal fluctuations within the right  $vAI_{seed}$  had less extensive connectivity with cortical regions, with connectivity largely in pgACC extending to dACC/paracingulate cortex, lateral OFC, posterior cingulate cortex, superior frontal gyrus, and medial FPA. At the subcortical level, intrinsic signal fluctuations within the right  $vAI_{seed}$  were correlated with signal fluctuations in ventral putamen, and substantia innominata.

Since maps at our a priori threshold of  $z(r) = 0.2$  did not reveal any target voxels in the amygdala, yet the amygdala is consistently engaged during affective experience (Lindquist et al., in press), we employed a region of interest approach to examine the dAI and vAI connectivity to amygdala at a reduced threshold of  $z(r) = 0.1$ . We selected this relatively low threshold to enable the identification of the subcortical regions which, compared to cortical regions, tend to have weaker low frequency BOLD signals (Cole et al., 2010). As predicted, intrinsic signal fluctuations within the right  $vAI_{seed}$ , but not within the right  $dAI_{seed}$ , correlated with signal fluctuations in the amygdala

(right amygdala coordinates: + 20, -4, -15,  $M_{z(r)} = 0.08$ ,  $SD_{z(r)} = 0.16$ ) (Figure S1 in supplemental material).

Although the two networks appeared topographically distinct, they did show some overlap (see Fig. 1 in purple). Regions of overlap between the two AI networks included right lateral OFC, bilateral vAI around the right  $vAI_{seed}$  and adjacent frontal operculum, bilateral dACC/paracingulate cortex as well as a small region in ventral putamen.

Tables 1 and 2 list the strength of connectivity between each insular seed region and network targets. As can be seen from data column 1, there was wide variation in the strength of connectivity between each  $AI_{seed}$  and the targets in the rest of its network. Amidst this variability, the average within-network correlations were significantly stronger than the between network correlations (see Table 3). Within-network correlation coefficients were significantly greater than between-network correlation coefficients as revealed by paired-sample *t*-tests [ $t(88) = 19.13$ ,  $p < 0.01$  for the  $dAI_{targets} - dAI_{seed}$  as compared to  $vAI_{targets} - vAI_{seed}$  connectivity and  $t(88) = 16.55$ ,  $p < 0.01$  for the  $vAI_{targets} - dAI_{seed}$  as compared to  $vAI_{targets} - vAI_{seed}$  connectivity]. In addition, the central

**Table 1**  
Means and standard deviations of correlation peaks between each  $AI_{seed}$  and the  $dAI_{targets}$ ,  $z(r) > 0.2$ .

| Label                                                                                | Peak coordinate | $z(r)$ |     |     |                          |                 |                          |                 |
|--------------------------------------------------------------------------------------|-----------------|--------|-----|-----|--------------------------|-----------------|--------------------------|-----------------|
|                                                                                      |                 | X      | Y   | Z   | Sample 1<br>( $n = 89$ ) |                 | Sample 2<br>( $n = 31$ ) |                 |
|                                                                                      |                 |        |     |     | $dAI_{seed}$             | $vAI_{seed}$    | $dAI_{seed}$             | $vAI_{seed}$    |
| Frontal Pole                                                                         | R               | 38     | 46  | 28  | 0.49<br>(0.25)           | 0.08<br>(0.20)  | 0.53<br>(0.25)           | 0.12<br>(0.26)  |
|                                                                                      | L               | -38    | 44  | 28  | 0.37<br>(0.24)           | 0.00<br>(0.20)  | 0.45<br>(0.24)           | 0.05<br>(0.20)  |
| Middle Frontal Gyrus                                                                 | R               | 40     | 32  | 36  | 0.29<br>(0.27)           | 0.13<br>(0.19)  | 0.18<br>(0.28)           | 0.09<br>(0.26)  |
|                                                                                      | L               | -36    | 34  | 36  | 0.26<br>(0.24)           | 0.04<br>(0.17)  | 0.29<br>(0.26)           | 0.00<br>(0.22)  |
| Precentral Gyrus                                                                     | R               | 52     | 6   | 36  | 0.30<br>(0.23)           | -0.04<br>(0.17) | 0.28<br>(0.25)           | -0.04<br>(0.23) |
|                                                                                      | L               | -58    | 6   | 10  | 0.35<br>(0.22)           | -0.05<br>(0.15) | 0.30<br>(0.23)           | 0.00<br>(0.19)  |
| Inferior Frontal Gyrus,<br>pars opercularis<br>Supplementary Motor Area              | R               | 56     | 16  | 10  | 0.45<br>(0.23)           | 0.10<br>(0.17)  | 0.47<br>(0.27)           | 0.10<br>(0.24)  |
|                                                                                      | R               | 4      | 4   | 54  | 0.34<br>(0.20)           | -0.04<br>(0.19) | 0.38<br>(0.29)           | 0.00<br>(0.18)  |
|                                                                                      | L               | -2     | 2   | 52  | 0.27<br>(0.20)           | -0.05<br>(0.17) | 0.27<br>(0.31)           | 0.03<br>(0.16)  |
| Frontal Operculum                                                                    | R               | 40     | 18  | 6   | 0.93<br>(0.22)           | 0.14<br>(0.16)  | 0.95<br>(0.29)           | 0.20<br>(0.25)  |
|                                                                                      | L               | -38    | 20  | 6   | 0.59<br>(0.26)           | 0.15<br>(0.16)  | 0.60<br>(0.27)           | 0.17<br>(0.24)  |
| Central Opercular Cortex                                                             | R               | 48     | 0   | 4   | 0.36<br>(0.20)           | 0.00<br>(0.17)  | 0.35<br>(0.22)           | 0.09<br>(0.18)  |
|                                                                                      | L               | -48    | 0   | 4   | 0.36<br>(0.20)           | 0.00<br>(0.16)  | 0.33<br>(0.25)           | 0.08<br>(0.22)  |
| Lateral Orbitofrontal Cortex                                                         | R               | 32     | 22  | -14 | 0.33<br>(0.19)           | 0.79<br>(0.21)  | 0.37<br>(0.24)           | 0.87<br>(0.28)  |
| Superior Parietal Lobule                                                             | R               | 42     | -46 | 60  | 0.28<br>(0.23)           | -0.06<br>(0.17) | 0.18<br>(0.29)           | 0.02<br>(0.21)  |
| Anterior Supramarginal Gyrus                                                         | R               | 58     | -30 | 48  | 0.37<br>(0.22)           | -0.05<br>(0.16) | 0.30<br>(0.22)           | -0.03<br>(0.23) |
|                                                                                      | L               | -58    | -36 | 42  | 0.31<br>(0.20)           | -0.05<br>(0.17) | 0.30<br>(0.27)           | -0.01<br>(0.23) |
| Posterior Supramarginal Gyrus                                                        | R               | 62     | -38 | 42  | 0.45<br>(0.24)           | 0.06<br>(0.18)  | 0.34<br>(0.24)           | 0.06<br>(0.26)  |
| Superior Temporal Pole                                                               | R               | 52     | 18  | -18 | 0.30<br>(0.24)           | 0.13<br>(0.18)  | 0.27<br>(0.28)           | 0.07<br>(0.18)  |
|                                                                                      | L               | -50    | 12  | -12 | 0.30<br>(0.24)           | 0.12<br>(0.20)  | 0.29<br>(0.26)           | 0.04<br>(0.22)  |
| Lateral Occipital                                                                    | R               | 14     | -72 | 52  | 0.21<br>(0.22)           | -0.05<br>(0.15) | 0.15<br>(0.28)           | -0.08<br>(0.22) |
| Anterior Mid Cingulate/Dorsal<br>Anterior Cingulate Cortex                           | R               | 4      | 20  | 32  | 0.45<br>(0.24)           | 0.19<br>(0.20)  | 0.54<br>(0.30)           | 0.18<br>(0.24)  |
|                                                                                      | L               | -2     | 16  | 32  | 0.36<br>(0.23)           | 0.14<br>(0.19)  | 0.40<br>(0.28)           | 0.14<br>(0.22)  |
| Paracingulate gyrus of Anterior<br>Mid Cingulate/Dorsal Anterior<br>Cingulate Cortex | R               | 4      | 16  | 46  | 0.59<br>(0.24)           | 0.14<br>(0.21)  | 0.48<br>(0.36)           | 0.17<br>(0.19)  |
|                                                                                      | L               | -2     | 14  | 46  | 0.44<br>(0.20)           | 0.08<br>(0.20)  | 0.39<br>(0.32)           | 0.07<br>(0.19)  |
| Posterior Cingulate Cortex                                                           | R               | 8      | -32 | 44  | 0.27<br>(0.24)           | 0.10<br>(0.17)  | 0.23<br>(0.36)           | 0.08<br>(0.19)  |
| Ventral Anterior Insula                                                              | R               | 40     | 14  | -8  | 0.62<br>(0.22)           | 0.26<br>(0.21)  | 0.64<br>(0.24)           | 0.21<br>(0.20)  |
|                                                                                      | L               | -40    | 12  | -8  | 0.48<br>(0.22)           | 0.31<br>(0.20)  | 0.57<br>(0.30)           | 0.21<br>(0.22)  |
| Dorsal Anterior Insula                                                               | L               | -40    | 0   | 2   | 0.45<br>(0.18)           | 0.03<br>(0.18)  | 0.42<br>(0.20)           | 0.07<br>(0.23)  |
| Ventral Mid Insula                                                                   | R               | 40     | 0   | -6  | 0.33<br>(0.19)           | 0.08<br>(0.19)  | 0.33<br>(0.16)           | 0.07<br>(0.25)  |
|                                                                                      | L               | -40    | 0   | -6  | 0.33<br>(0.19)           | 0.08<br>(0.18)  | 0.36<br>(0.18)           | 0.09<br>(0.25)  |
| Dorsal Mid Insula                                                                    | R               | 40     | 0   | 4   | 0.41<br>(0.19)           | -0.02<br>(0.17) | 0.37<br>(0.23)           | 0.11<br>(0.24)  |
|                                                                                      | L               | -38    | 0   | 6   | 0.46<br>(0.19)           | -0.01<br>(0.17) | 0.43<br>(0.22)           | 0.08<br>(0.27)  |
| Posterior Insula                                                                     | R               | 40     | -10 | -6  | 0.29<br>(0.20)           | 0.07<br>(0.18)  | 0.27<br>(0.20)           | 0.05<br>(0.23)  |
|                                                                                      | L               | -40    | -4  | -8  | 0.23<br>(0.17)           | 0.06<br>(0.18)  | 0.28<br>(0.19)           | 0.03<br>(0.25)  |
| Putamen                                                                              | R               | 22     | 12  | -2  | 0.24<br>(0.15)           | 0.17<br>(0.17)  | 0.24<br>(0.16)           | 0.20<br>(0.21)  |

**Table 2**  
Means and standard deviations of correlation peaks between each  $AI_{seed}$  and the  $vAI_{targets}$ ,  $z(r) > 0.2$ .

| Label                                                   | Peak coordinate |     |     | $z(r)$               |                 |                      |                 |                |
|---------------------------------------------------------|-----------------|-----|-----|----------------------|-----------------|----------------------|-----------------|----------------|
|                                                         |                 |     |     | Sample 1<br>(n = 89) |                 | Sample 2<br>(n = 31) |                 |                |
|                                                         |                 |     |     | $dAI_{seed}$         | $vAI_{seed}$    | $dAI_{seed}$         | $vAI_{seed}$    |                |
| Frontal Pole                                            | R               | 22  | 54  | 28                   | 0.08<br>(0.29)  | 0.25<br>(0.21)       | 0.11<br>(0.32)  | 0.16<br>(0.22) |
| Superior Frontal Gyrus                                  | R               | 4   | 28  | 56                   | 0.15<br>(0.22)  | 0.22<br>(0.20)       | 0.02<br>(0.26)  | 0.17<br>(0.29) |
| Lateral Orbitofrontal Cortex                            | R               | 26  | 18  | -18                  | 0.08<br>(0.20)  | 1.04<br>(0.28)       | 0.14<br>(0.24)  | 1.25<br>(0.27) |
|                                                         | L               | -30 | 16  | -18                  | 0.00<br>(0.21)  | 0.47<br>(0.20)       | 0.10<br>(0.26)  | 0.54<br>(0.30) |
| Pregenua Anterior Cingulate Cortex                      | R               | 2   | 36  | 16                   | 0.11<br>(0.19)  | 0.35<br>(0.17)       | 0.07<br>(0.25)  | 0.20<br>(0.21) |
|                                                         | L               | -2  | 36  | 16                   | 0.09<br>(0.22)  | 0.33<br>(0.17)       | 0.07<br>(0.27)  | 0.18<br>(0.19) |
| Paracingulate Gyrus of Dorsal Anterior Cingulate Cortex | R               | 2   | 40  | 26                   | 0.06<br>(0.26)  | 0.41<br>(0.21)       | 0.00<br>(0.27)  | 0.31<br>(0.23) |
|                                                         | L               | -2  | 38  | 26                   | 0.10<br>(0.23)  | 0.38<br>(0.20)       | 0.05<br>(0.28)  | 0.28<br>(0.21) |
| Posterior Cingulate Cortex                              | R               | 4   | -22 | 40                   | -0.02<br>(0.23) | 0.27<br>(0.17)       | -0.02<br>(0.19) | 0.17<br>(0.20) |
|                                                         | L               | -2  | -20 | 34                   | -0.06<br>(0.18) | 0.24<br>(0.17)       | -0.11<br>(0.21) | 0.21<br>(0.19) |
| Ventral Anterior Insula                                 | L               | -38 | 14  | -10                  | 0.41<br>(0.22)  | 0.41<br>(0.19)       | 0.52<br>(0.26)  | 0.28<br>(0.21) |
|                                                         | R               | 18  | 8   | -8                   | 0.22<br>(0.14)  | 0.27<br>(0.17)       | 0.26<br>(0.16)  | 0.30<br>(0.22) |
| Putamen                                                 | L               | -18 | 6   | -8                   | 0.15<br>(0.13)  | 0.23<br>(0.15)       | 0.19<br>(0.17)  | 0.23<br>(0.20) |
|                                                         | R               | 17  | 5   | -10                  | 0.17<br>(0.14)  | 0.26<br>(0.15)       | 0.22<br>(0.22)  | 0.30<br>(0.24) |

tendencies of the distributions of within- and between-network connectivity were non-overlapping, further demonstrating that the two networks are distinct (Fig. 2).

The summary connectivity indices for each network are computed as follows: a) a dAI-to-dACC/paracingulate connectivity measure of  $z(r)$  values between the  $dAI_{seed}$  and its target region in dACC/paracingulate cortex (right dACC/paracingulate coordinates: + 4, 16, 46; left dACC/paracingulate coordinates: + -2, 14, 46); b) a dAI-to-fronto-parietal ROIs connectivity measure of  $z(r)$  values between the  $dAI_{seed}$  and its target sites in or around the dACC/paracingulate (right dACC/paracingulate coordinates: + 4, 16, 46; left dACC/paracingulate coordinates: + -2, 14, 46), MFG (right MFG coordinates: + 40, 32, 46; left MFG coordinates: + -36, 34, 36), and SMG (right anterior SMG coordinates: + 58, -30, 48; left anterior SMG coordinates: + -58, -36, 42); and c) a  $dAI_{seed}$ -to- $dAI_{target}$  ROIs connectivity measure of  $z(r)$  values between the  $dAI_{seed}$  and all of its target regions. Correspondingly, for the vAI network we calculated the following measures: a) a vAI-to-pgACC connectivity measure of  $z(r)$  values between the  $vAI_{seed}$  and its target region in pgACC (right pgACC coordinates: + 2, 36, 16; left pgACC coordinates: + -2, 36, 16); b) a vAI-to-fronto-limbic-striatal ROIs connectivity measure of  $z(r)$  values between the  $vAI_{seed}$  region and target sites in or around the FPA (right FPA coordinates: + 22, 54, 28), pgACC (right pgACC coordinates: + 2, 36, 16; left pgACC coordinates: + -2, 36, 16), and ventral striatum (right ventral putamen coordinates: + 18, 8, -8; left ventral putamen coordinates: + -18, 6, -8); and c) a  $vAI_{seed}$ -to- $vAI_{targets}$  connectivity measure of  $z(r)$  values between the  $vAI_{seed}$  and all of its target regions. The means and standard deviations of the summary connectivity measures for the dAI and vAI network in Sample 1 are shown in Table 3 (data columns 1 and 2 and Figure S2 in supplemental material). As predicted, the within-network summary connectivity measures were higher than the summary measures of between-network connectivity.

Reliability of the right dAI and right vAI networks

Using the regions of interest defined in Sample 1, we estimated the reliability of the right dAI and right vAI networks in Sample 2. As expected, every index we computed demonstrated the stability of the right dAI and right vAI networks in our second independent sample of participants. The connectivity maps for Sample 2 were highly similar to those maps for Sample 1 (Fig. 3). The correlation coefficients between  $AI_{targets}$  and  $AI_{seeds}$  are presented in Tables 1 and 2, columns 3 and 4. The average within-network correlations were significant stronger than the between-network correlations (see Table 3) [ $t(31) = 9.57, p < 0.01$  for the  $dAI_{targets}$ - $dAI_{seed}$  as compared to  $dAI_{targets}$ - $vAI_{seed}$ ;  $t(31) = 8.65, p < 0.01$  for the  $vAI_{targets}$ - $dAI_{seed}$  as compared to  $vAI_{targets}$ - $vAI_{seed}$ ]. As in Sample 1, the central tendencies of distributions of within- and between-network connectivity in Sample 2 were non-overlapping (Fig. 2). The three summary connectivity measures described above were very similar in the two samples (Table 3; Fig. 4; Figure S2). These results support the generalizability of the observations that the two networks are reliably distinct from each other regardless of exactly how the strength of connectivity is computed. Most importantly, the intraclass correlation coefficients (ICC) demonstrated high reliability for the right dAI network (ICC = 0.97, two-way random effects,  $p < 0.01$ ) and the right vAI network (ICC = 0.95, two-way random effects,  $p < 0.01$ ) across the two samples.

As with Sample 1, we reduced the threshold from  $z(r) = 0.2$  to  $z(r) = 0.1$  to examine amygdala connectivity within the two networks. Replicating Sample 1, the amygdala was weakly connected to the right vAI network ( $M_{z(r)} = 0.07, SD_{z(r)} = 0.19$ ). In addition, however, the amygdala showed weak connectivity within the right dAI network in Sample 2 ( $M_{z(r)} = 0.06, SD_{z(r)} = 0.22$ ) (see supplemental material Figure S1 and page 1 for discussion).

The relation between strength of connectivity and behavior

As predicted, the strength of connectivity between each  $AI_{seed}$  and its major connection in the ACC was moderately and specifically related to the behavioral variables (see Table 4). Scatterplots of these results are presented in Fig. 5. The means and standard deviations of the behavioral measures are shown in Table S1 in supplemental material. Consistent with our hypotheses, individuals with stronger connectivity within the dAI network performed faster on Trail Making

**Table 3**  
Means and standard deviations of the three summary connectivity measures for the dAI and vAI networks,  $z(r) > 0.20$ .

| Metric of connectivity                                                                              | $z(r)$               |                |                      |                |
|-----------------------------------------------------------------------------------------------------|----------------------|----------------|----------------------|----------------|
|                                                                                                     | Sample 1<br>(n = 89) |                | Sample 2<br>(n = 31) |                |
|                                                                                                     | $dAI_{seed}$         | $vAI_{seed}$   | $dAI_{seed}$         | $vAI_{seed}$   |
| <i>dAI network summary connectivity measures</i>                                                    |                      |                |                      |                |
| $dAI_{seed}$ - bilateral dACC/paracingulate                                                         | 0.52<br>(0.21)       | 0.11<br>(0.20) | 0.43<br>(0.33)       | 0.12<br>(0.18) |
| $dAI_{seed}$ - bilateral targets in dACC/paracingulate, middle frontal gyri, and supramarginal gyri | 0.37<br>(0.15)       | 0.05<br>(0.13) | 0.32<br>(0.19)       | 0.05<br>(0.14) |
| $dAI_{seed}$ - all bilateral $dAI_{targets}$                                                        | 0.38<br>(0.22)       | 0.08<br>(0.18) | 0.38<br>(0.25)       | 0.10<br>(0.22) |
| <i>vAI network summary connectivity measures</i>                                                    |                      |                |                      |                |
| $vAI_{seed}$ - bilateral pgACC                                                                      | 0.10<br>(0.20)       | 0.34<br>(0.17) | 0.07<br>(0.25)       | 0.19<br>(0.19) |
| $vAI_{seed}$ -right frontal pole, bilateral targets in pgACC, and ventral putamen                   | 0.13<br>(0.13)       | 0.28<br>(0.11) | 0.14<br>(0.15)       | 0.22<br>(0.12) |
| $vAI_{seed}$ - all bilateral $vAI_{targets}$                                                        | 0.11<br>(0.20)       | 0.37<br>(0.19) | 0.12<br>(0.24)       | 0.33<br>(0.23) |

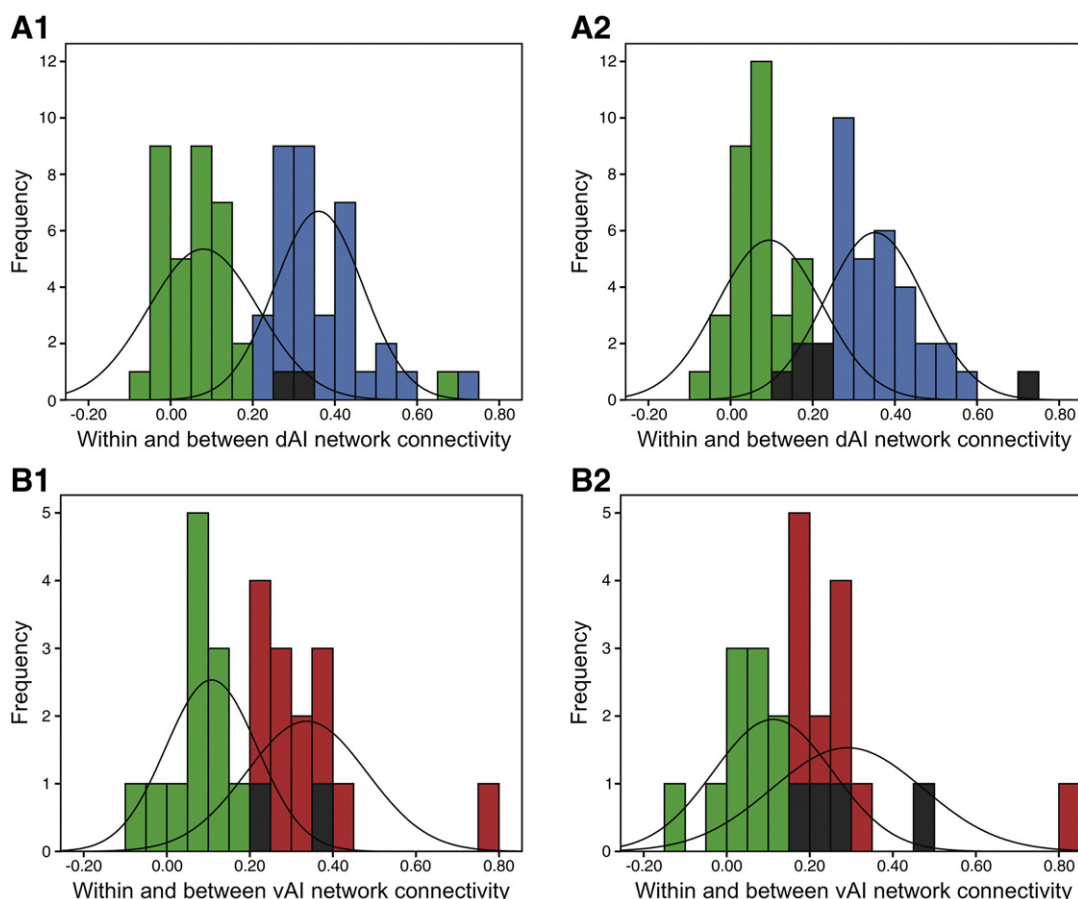


**Fig. 2.** The distributions of within- and between-network connectivity for each ROI pair in both samples. The central tendencies of the connectivity distributions between the right dAI<sub>seed</sub> and the dAI<sub>targets</sub> (blue) and between the right vAI<sub>seed</sub> and the dAI<sub>targets</sub> (green) in Sample 1 (A1) and Sample 2 (A2) are not overlapping. Similarly, the central tendencies of the connectivity distributions between the right vAI<sub>seed</sub> and the vAI<sub>targets</sub> (red) and between the right dAI<sub>seed</sub> and the vAI<sub>targets</sub> (green) are non-overlapping in Sample 1 (B1) and Sample 2 (B2). ROI pairs that are present in both the right dAI and right vAI networks are indicated in shaded bars. (For interpretation of the references to color in this figure legend, the reader is referred to the web version of this article.)

Test A and Trail B but did not have stronger subjective experiences of arousal when viewing evocative negative images. The strength of connectivity between the dAI and dACC/paracingulate cortex explained 16% of the variance in Trail Making Test B time ( $r = -0.40$ ,  $p < 0.05$ ) but only 4% of the variance in arousal ratings to evocative images ( $r = 0.20$ ,  $p = 0.30$ ) (see also supplemental material).

In contrast, individuals with stronger connectivity within the right vAI network had more intense subjective experiences of arousal when viewing evocative negative images but did not perform faster on Trail Making Test. The strength of connectivity between the vAI and pgACC explained 20% of the variance in arousal ratings to negative pictures ( $r = 0.45$ ,  $p < 0.05$ ) as opposed to 2% of the variance in Trail Making Test B time ( $r = -0.14$ ,  $p = 0.51$ ).

There was no relationship between vAI-pgACC connectivity and arousal ratings to positive pictures. It has been suggested that there are lateralization differences in positive and negative affect involving the AI and ACC, such that the right AI-ACC connection is preferentially involved in negative feelings associated with sympathetic activity increase whereas the left AI-ACC connection is preferentially involved in positive feelings associated with parasympathetic increase (Craig, 2005). To explore this possibility we performed a post hoc intrinsic connectivity analysis using a left vAI seed (left vAI coordinates: -28, 17, -15) and examined whether left vAI connectivity predicted the intensity of positive affective experience (see page 1 in the supplemental material). Our results showed that the strength of connectivity between the left vAI and its major connection in ACC was significantly related to the intensity of subjective arousal experiences in response

to negative but not positive pictures (see supplemental material Table S2 and page 1).

Although the correlations between behavioral measures and other dAI and vAI connectivity measures did not reach conventional levels of significance, all were in the hypothesized directions (see Table 4).

## Discussion

### *The distinct topographic anatomy of right dAI vs. right vAI large-scale networks*

Two prior studies are particularly relevant to the present results, since they compared dAI versus vAI intrinsic connectivity using rs-fcMRI (Deen et al., 2011; Nelson et al., 2010). Our results on the topography of the networks are largely similar to theirs with a few key differences. The right dAI network we identified comprised dACC, rostral dorsolateral prefrontal, rostral inferior parietal, and dorsal striatal regions. The dAI networks identified in the prior studies—which focused specifically on corticocortical connectivity—were remarkably similar (Deen et al., 2011; Nelson et al., 2010). The right vAI network we identified comprised pgACC, OFC and ventral striatal regions. The vAI networks identified in the prior studies were also very similar, although they both found small inferior parietal and superior temporal regions that we did not observe. Furthermore, it is not clear in those papers whether OFC regions were identified. These slight differences are likely related to differences in the placement of seeds, statistical thresholds used to identify correlated regions, and possibly also differences in processing algorithms.

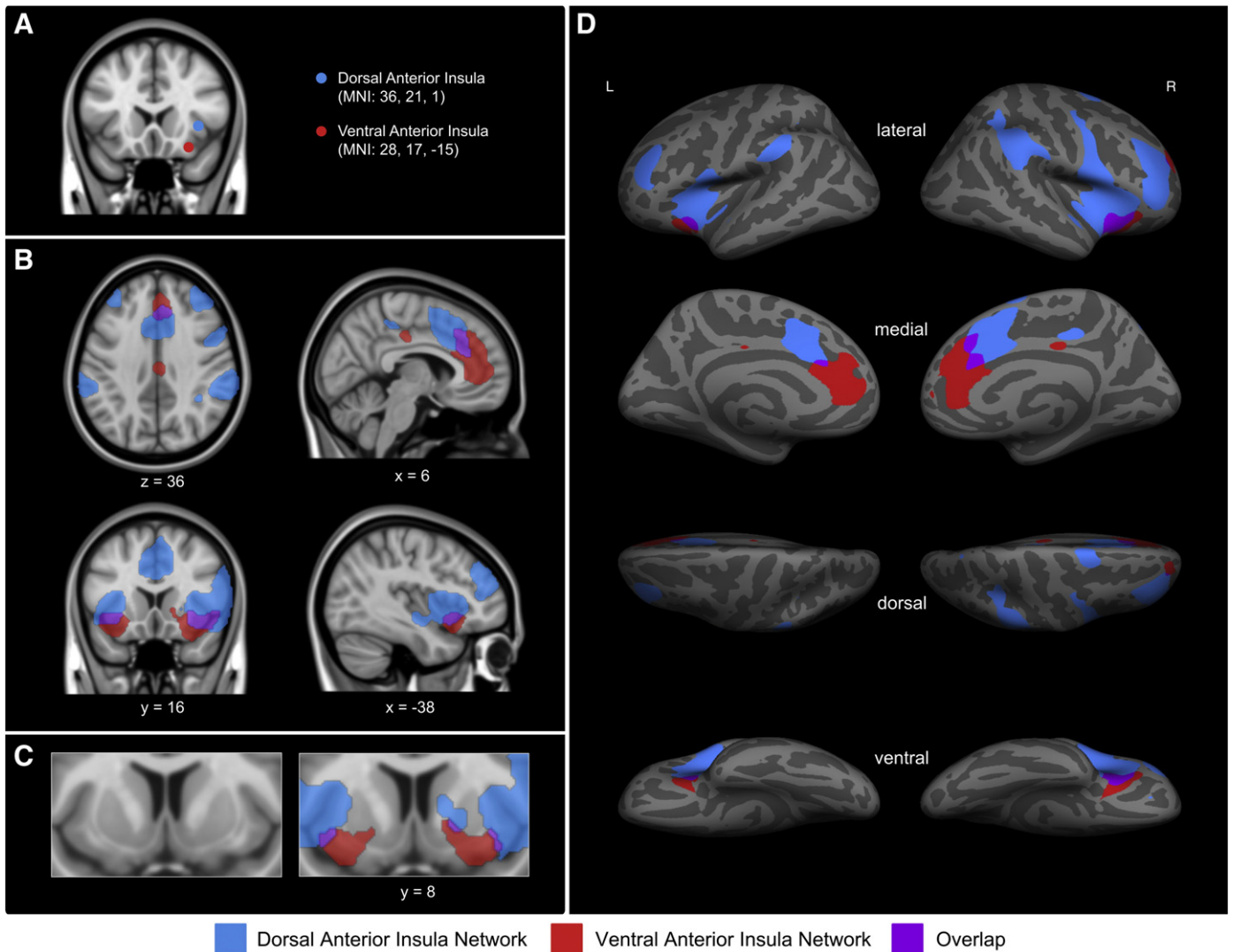


**Fig. 3.** The confirmatory analysis performed using Sample 2 shows that the (A) right dAI<sub>seed</sub> and right vAI<sub>seed</sub> (shown in blue and red, respectively) have distinct patterns of intrinsic functional connectivity at  $z(r) > 0.2$ ; (B and C) regions that preferentially correlate with right dAI<sub>seed</sub> are shown in blue, regions that preferentially correlate with right vAI<sub>seed</sub> are shown in red, and regions that correlate with both seeds are shown in purple; (D) the distinct patterns of connectivity of the right dAI<sub>seed</sub> and right vAI<sub>seed</sub> at  $z(r) > 0.2$  are displayed on the lateral and medial inflated surfaces of the left and right hemisphere. Details of the method of display are the same as in Fig. 1. (For interpretation of the references to color in this figure legend, the reader is referred to the web version of this article.)

The “salience” network identified by Seeley et al. (2007) was anchored in the “orbital frontoinsula” (in a location slightly more lateral, anterior, and dorsal than our vAI) and was largely similar topographically but also included MFG and supplementary motor area, regions that in our study were preferentially correlated with the right dAI seed. The executive control network identified in that prior study was also largely similar topographically to our right dAI network, primarily centered around dorsolateral frontoparietal regions as well as dorsomedial prefrontal/paracingulate cortex. Interestingly, the executive control network in that prior study included a dAI node slightly rostral to ours when the data were analyzed using a seed-based method similar to ours (employing a dorsolateral prefrontal seed) but when independent component analysis was used this network included a much more ventral (orbital frontoinsula) node. There were several similar areas of convergence between the networks, particularly in frontoinsula/opercular and anterior cingulate/paracingulate cortex.

The results reported here also extend previous findings to show dorsoventral variation in AI connectivity to subcortical regions. The right dAI network was connected to dorsal putamen whereas the right vAI region was connected with ventral putamen, substantia

innominata and to a lesser degree with the amygdala. These findings for the right vAI are largely similar to those reported by Seeley et al. (2007), except that we found slightly more variable brainstem connectivity (Figure S3 in supplemental material).

In sum, our findings on the topography of the distinct right AI networks are consistent with prior functional connectivity data. They are also very similar to tract tracing data from non-human primate studies (Augustine, 1996; Mesulam and Mufson, 1982a, b) and diffusion tensor imaging data from humans (Cerliani et al., 2011) showing preferential connections for the dAI with areas in prefrontal cortex, precentral operculum, and parietal cortex and for the vAI with areas in limbic and paralimbic structures.

#### *The distinct behavioral correlates of right dAI vs. right vAI large-scale networks*

The major novel contribution of the present study is the demonstration of a behavioral dissociation between the right dAI and right vAI networks: individual differences in the right dAI connectivity relate to individual differences in attention and processing speed whereas individual differences in the right vAI connectivity relate to the intensity

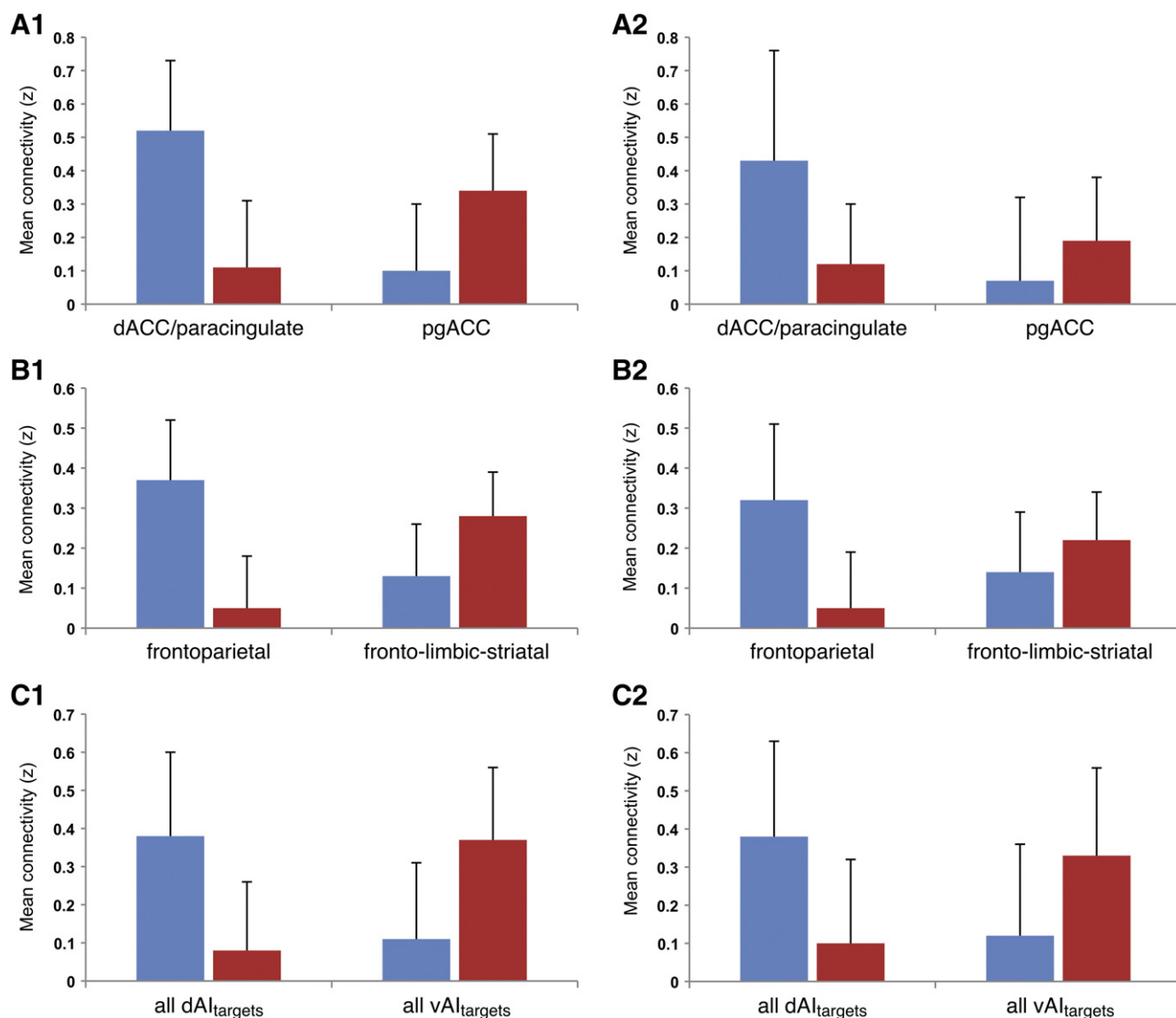


**Fig. 4.** The three summary connectivity measures within the right dAI network (blue) and the right vAI network (red). The within network correlation coefficients are higher than the between network correlation coefficients as demonstrated by the connectivity measures in Sample 1 (A1, B1, and C1) and in Sample 2 (A2, B2, and C2). (For interpretation of the references to color in this figure legend, the reader is referred to the web version of this article.)

of on-line affective experience in response to negative images. The prior two studies on dAI vs. vAI networks have demonstrated that both the dAI and the vAI are engaged during task performance in response to disgusting images (Deen et al., 2011) and to images being gradually revealed (thought to represent attentional or control processes) (Nelson et al., 2010), but did not demonstrate behavioral dissociations between the regions themselves or the larger networks.

We found that the strength of connectivity between the dAI-dACC nodes of the right dAI network was associated with performance on Trail Making Test B and Trail Making Test A but not with subjective arousal ratings to negative evocative images. Trail Making Test A is a task requiring processing speed, visual search, motor control, and attention; Trail Making Test B adds an additional component of set-shifting (Strauss et al., 2006). This finding is generally similar to that reported by Seeley et al. (2007) for their executive control network, which demonstrated a resting-state functional connectivity correlation with performance on the Trail Making Test, although their localization of this effect was in the lateral parietal cortex. This finding is also highly consistent with a task-related fMRI study (Sridharan et al., 2008) showing that a

network comprising the right fronto-insula and dACC is involved in switching between the central executive network and the default mode network. Our right dAI network is similar to other intrinsic networks, most notably the “ventral attention” (Corbetta and Shulman, 2002), the “basal ganglia-fronto-insula” (Shulman et al., 2009), the “cingulo-operculum control” (Dosenbach et al., 2007; Nelson et al., 2010) and the “frontoparietal control” networks (Vincent et al., 2008). Task-related fMRI studies have shown increases in the activity of many regions within dAI network (dACC, MFG, SMG, FPA) during tasks that require attention/executive function (Barch et al., 1997; Cole and Schneider, 2007; Corbetta and Shulman, 2002; Dodds et al., 2011; Eichele et al., 2008; Kaller et al., 2011). Furthermore, a number of task-related fMRI studies have highlighted the role of the dAI and dACC in attention, including tonic alertness (Sadaghiani et al., 2010), stimulus-driven shifts of attention toward unexpected stimuli (Corbetta and Shulman, 2002; Corbetta et al., 2008; Downar et al., 2002; Shulman et al., 2009), top-down control signals (Cole and Schneider, 2007) related to initiation, task-set maintenance, feedback (Dosenbach et al., 2006, 2008), mind wandering (Mason et al., 2007) and momentary lapses

**Table 4**  
Pearson correlations between the behavioral measures and the three summary connectivity measures for the dAI and vAI networks,  $z(r) > 0.20$ .

|                                                                                                            | Trails A Time           | Trails B Time            | Arousal Rating to Negative Images | Arousal Rating to Positive Images |
|------------------------------------------------------------------------------------------------------------|-------------------------|--------------------------|-----------------------------------|-----------------------------------|
| <i>dAI network summary connectivity measures</i>                                                           |                         |                          |                                   |                                   |
| dAI <sub>seed</sub> – bilateral dACC/paracingulate                                                         | -0.41<br>( $p = 0.04$ ) | -0.40<br>( $p = 0.05$ )  | 0.20<br>( $p = 0.30$ )            | -0.05<br>( $p = 0.79$ )           |
| dAI <sub>seed</sub> – bilateral targets in dACC/paracingulate, middle frontal gyri, and supramarginal gyri | -0.29<br>( $p = 0.17$ ) | -0.19<br>( $p = 0.37$ )  | 0.09<br>( $p = 0.63$ )            | 0.03<br>( $p = 0.86$ )            |
| dAI <sub>seed</sub> – all bilateral dAI <sub>targets</sub>                                                 | -0.38<br>( $p = 0.06$ ) | -0.024<br>( $p = 0.26$ ) | 0.11<br>( $p = 0.58$ )            | -0.13<br>( $p = 0.48$ )           |
| <i>vAI network summary connectivity measures</i>                                                           |                         |                          |                                   |                                   |
| vAI <sub>seed</sub> – bilateral pgACC                                                                      | -0.02<br>( $p = 0.92$ ) | -0.14<br>( $p = 0.51$ )  | 0.45<br>( $p = 0.01$ )            | 0.18<br>( $p = 0.34$ )            |
| vAI <sub>seed</sub> – right frontal pole, bilateral targets in pgACC, and ventral putamen                  | 0.05<br>( $p = 0.82$ )  | -0.01<br>( $p = 0.98$ )  | 0.25<br>( $p = 0.19$ )            | 0.19<br>( $p = 0.33$ )            |
| vAI <sub>seed</sub> – all bilateral vAI <sub>targets</sub>                                                 | -0.09<br>( $p = 0.69$ ) | -0.02<br>( $p = 0.93$ )  | 0.23<br>( $p = 0.22$ )            | 0.13<br>( $p = 0.51$ )            |

in attention (Weissman et al., 2006) as well as in motor programming (Schulz et al., 2011). The current study extends these findings by showing that, in the absence of a task, individual differences in connectivity strength within the dAI-dACC system predict individual differences in attention and processing speed.

We also found that the strength of vAI-pgACC connectivity was preferentially associated with momentary experiences of arousal in

response to evocative negative pictures, but not with performance on Trail Making Test. These results extend the findings of Seeley et al. (2007) who reported that the strength of ACC connectivity (a region near our pgACC node) within their salience network predicted self-reported anxiety prior to MRI scanning. Momentary experiences of arousal are integral to subjective feelings experienced across affective, cognitive, or physical task domains (Barrett et al., 2004; Craig, 2002,

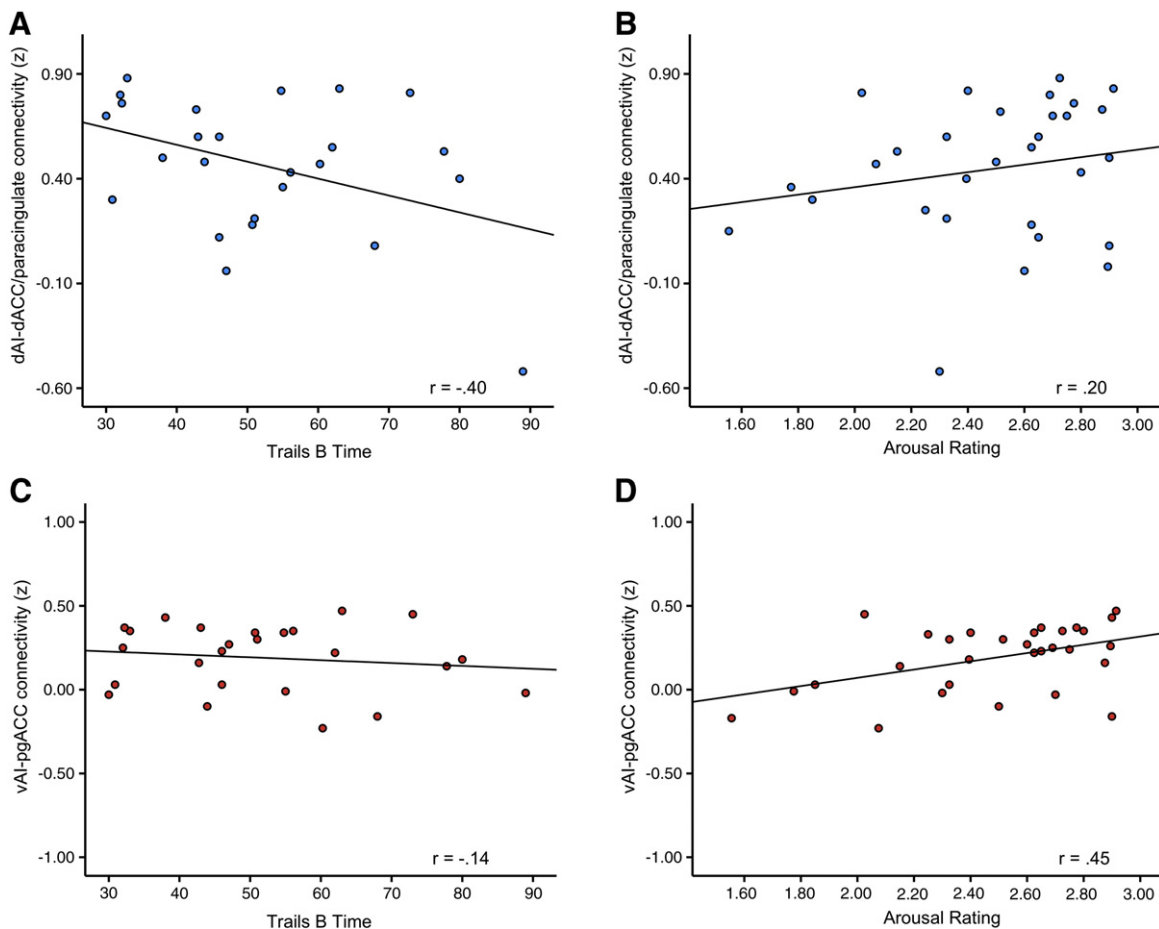


**Fig. 5.** Behavioral correlates of the strength of connectivity within right dAI and right vAI networks. The strength of connectivity between right dAI<sub>seed</sub> and its target region in dACC/paracingulate region correlated inversely with (A) Trail Making Test B Time ( $p < 0.05$ ) but not with arousal ratings to evocative negative images ( $p = 0.3$ ). The strength of connectivity between right vAI<sub>seed</sub> and its target region in pgACC region had no relationship with (C) Trail Making Test B Time ( $p = 0.51$ ) but, instead, correlated directly with (D) the arousal ratings to evocative negative images ( $p < 0.05$ ).

2009). Our work extends knowledge of the vAI's role in affective experience and fits well with previous functional neuroimaging work. Our right vAI network includes pgACC, OFC, ventral striatum that are routinely active during tasks probing affect and emotion (Barrett and Bliss-Moreau, 2009; Bartels and Zeki, 2004; Damasio et al., 2000; Heining et al., 2003; Kober et al., 2008; Lindquist et al., in press; Phan et al., 2004; Small et al., 2001; Wager et al., 2008). Our findings are also consistent with task-related fMRI studies reporting that both vAI and vACC commonly increase their activity during interoceptive processing (Gu et al., 2010; Hua et al., 2005; Mutschler et al., 2009; Nagai et al., 2004) and in response to affectively arousing pictures (Craig, 2009; Weierich et al., 2010). The present findings further support the concept that vAI-pgACC processing might act as a filter to represent feelings in awareness (Allman et al., 2011; Craig, 2011).

#### Implications for Understanding Affect and Cognition

It has been long suggested (Goldman-Rakic, 1988; Mesulam, 1998) and demonstrated with imaging studies (LaBar et al., 2001; Seeley et al., 2007) that cognitive operations related to goal-oriented attention and executive function on the one hand, and affective value on the other, are integrated in certain key association and paralimbic cortical areas including the AI. One way to understand the present results is that both AI networks contribute to the processing of salient information, albeit somewhat differently. Consistent with models that postulate the involvement of the dAI-dACC system in integrating top-down and bottom-up salient information (Crottaz-Herbette and Menon, 2006; Eckert et al., 2009; Menon and Uddin, 2010), the dAI and dACC nodes through their connections with other parts of the right dAI network are well positioned to regulate goal-driven attention (Menon and Uddin, 2010), enhancing the activation of task-relevant and suppressing task-irrelevant networks (Spreng et al., 2010; Sridharan et al., 2008) to process whatever information is most relevant to the goal at hand. In contrast, the vAI and pgACC nodes, through their connections with other parts of the right vAI network, contribute to salience processing via affect, by contributing to the generation and interpretation of bodily feelings, so that an individual becomes aware of the value of information in the context of present needs or goals. Although distinct aspects of salience processing seem to be preferentially subserved within these two different networks, their activity ultimately converges through overlapping regions in AI, OFC, and ACC/paracingulate cortex as part of the larger attentional matrix to “sculpt sensory experience into a subjective landscape” (Mesulam, 1998). Future research should investigate both the intrinsic and dynamic coupling within and between these networks to better understand how distinct aspects of salience processing are optimally balanced to enable great achievement or are disrupted in neuropsychiatric illnesses.

#### Conclusions

Using rs-fcMRI, we showed that the human right dAI and right vAI anchor topographically distinct large-scale distributed brain networks. Our findings are consistent with several prior studies (Britz et al., 2010; Cauda et al., 2011; Deen et al., 2011; Nelson et al., 2010; Seeley et al., 2007; Taylor et al., 2009) and extend them by providing additional detail regarding the subcortical connectivity of these two networks. Most importantly, however, we demonstrated here that these two networks have dissociable behavioral correlates with the right dAI network relating to attention and processing speed and the right vAI network relating to intensity of affective experience.

#### Conflicts of interest

No conflicts of interest, financial or otherwise, are declared by the authors.

#### Acknowledgments

We thank Randy Buckner for providing the data used in the analysis of Sample 1 and the preprocessing/rs-fcMRI tools and Rebecca Dautoff for assistance. This work was supported by the National Institutes of Health Director's Pioneer Award (DP1OD003312) to Lisa Feldman Barrett, a National Institute on Aging grant (AG030311) to Lisa Feldman Barrett, a National Institute on Aging grant (AG029840) to Brad Dickerson, and the Shared Instrumentation Grants (1S1ORR023401, 1S1ORR019307, and 1S1ORR023043) from the National Center For Research Resources. The content is solely the responsibility of the authors and does not necessarily represent the official views of the National Center For Research Resources, the National Institutes of Health, or the National Institute on Aging.

#### Appendix A. Supplementary data

Supplementary data to this article can be found online at [doi:10.1016/j.neuroimage.2012.02.012](https://doi.org/10.1016/j.neuroimage.2012.02.012).

#### References

- Allman, J.M., Tetreault, N.A., Hakeem, A.Y., Manaye, K.F., Semendeferi, K., Erwin, J.M., Park, S., Goubert, V., Hof, P.R., 2011. The von Economo neurons in the frontoinsula and anterior cingulate cortex. *Ann. N. Y. Acad. Sci.* 1225, 59–71.
- Augustine, J.R., 1996. Circuitry and functional aspects of the insular lobe in primates including humans. *Brain Res. Brain Res. Rev.* 22, 229–244.
- Banzett, R.B., Mulnier, H.E., Murphy, K., Rosen, S.D., Wise, R.J., Adams, L., 2000. Breathlessness in humans activates insular cortex. *Neuroreport* 11, 2117–2120.
- Barch, D.M., Braver, T.S., Nystrom, L.E., Forman, S.D., Noll, D.C., Cohen, J.D., 1997. Dissociating working memory from task difficulty in human prefrontal cortex. *Neuropsychologia* 35, 1373–1380.
- Barrett, L.F., Bliss-Moreau, E., 2009. Affect as a Psychological Primitive. *Adv. Exp. Soc. Psychol.* 41, 167–218.
- Barrett, L.F., Quigley, K.S., Bliss-Moreau, E., Aronson, K.R., 2004. Interoceptive sensitivity and self-reports of emotional experience. *J. Personal. Soc. Psychol.* 87, 684–697.
- Bartels, A., Zeki, S., 2004. The neural correlates of maternal and romantic love. *NeuroImage* 21, 1155–1166.
- Biswal, B., Yetkin, F.Z., Haughton, V.M., Hyde, J.S., 1995. Functional connectivity in the motor cortex of resting human brain using echo-planar MRI. *Magn. Reson. Med.* 34, 537–541.
- Britz, J., Van De Ville, D., Michel, C.M., 2010. BOLD correlates of EEG topography reveal rapid resting-state network dynamics. *NeuroImage* 52, 1162–1170.
- Brooks, J.C., Zambreanu, L., Godinez, A., Craig, A.D., Tracey, I., 2005. Somatotopic organization of the human insula to painful heat studied with high resolution functional imaging. *NeuroImage* 27, 201–209.
- Buckner, R.L., 2010. Human functional connectivity: new tools, unresolved questions. *Proceedings of the National Academy of Sciences of the United States of America* 107, 10769–10770.
- Cauda, F., D'Agata, F., Sacco, K., Duca, S., Geminiani, G., Vercelli, A., 2011. Functional connectivity of the insula in the resting brain. *NeuroImage* 55, 8–23.
- Cerliani, L., Thomas, R.M., Jbabdi, S., Siero, J.C., Nanetti, L., Crippa, A., Gazzola, V., D'Arceuil, H., Keysers, C., 2011. Probabilistic tractography recovers a rostrocaudal trajectory of connectivity variability in the human insular cortex. *Hum. Brain Mapp* doi:10.1002/hbm.21338.
- Cole, M.W., Schneider, W., 2007. The cognitive control network: Integrated cortical regions with dissociable functions. *NeuroImage* 37, 343–360.
- Cole, M.W., Pathak, S., Schneider, W., 2010. Identifying the brain's most globally connected regions. *NeuroImage* 49, 3132–3148.
- Corbetta, M., Shulman, G.L., 2002. Control of goal-directed and stimulus-driven attention in the brain. *Nat. Rev. Neurosci.* 3, 201–215.
- Corbetta, M., Patel, G., Shulman, G.L., 2008. The reorienting system of the human brain: from environment to theory of mind. *Neuron* 58, 306–324.
- Craig, A.D., 2002. How do you feel? Interoception: the sense of the physiological condition of the body. *Nat. Rev. Neurosci.* 3, 655–666.
- Craig, A.D., 2005. Forebrain emotional asymmetry: a neuroanatomical basis? *Trends Cogn. Sci.* 9, 566–571.
- Craig, A.D., 2009. How do you feel—now? The anterior insula and human awareness. *Nat. Rev. Neurosci.* 10, 59–70.
- Craig, A.D., 2011. Significance of the insula for the evolution of human awareness of feelings from the body. *Ann. N. Y. Acad. Sci.* 1225, 72–82.
- Craig, A.D., Chen, K., Bandy, D., Reiman, E.M., 2000. Thermosensory activation of insular cortex. *Nat. Neurosci.* 3, 184–190.
- Critchley, H.D., 2009. Psychophysiology of neural, cognitive and affective integration: fMRI and autonomic indicators. *Int. J. Psychophysiol.* 73, 88–94.
- Critchley, H.D., Wiens, S., Rotshtein, P., Ohman, A., Dolan, R.J., 2004. Neural systems supporting interoceptive awareness. *Nat. Neurosci.* 7, 189–195.
- Critchley, H.D., Rotshtein, P., Nagai, Y., O'Doherty, J., Mathias, C.J., Dolan, R.J., 2005. Activity in the human brain predicting differential heart rate responses to emotional facial expressions. *NeuroImage* 24, 751–762.

- Crottaz-Herbette, S., Menon, V., 2006. Where and when the anterior cingulate cortex modulates attentional response: combined fMRI and ERP evidence. *J. Cogn. Neurosci.* 18, 766–780.
- Damasio, A.R., Grabowski, T.J., Bechara, A., Damasio, H., Ponto, L.L., Parvizi, J., Hichwa, R.D., 2000. Subcortical and cortical brain activity during the feeling of self-generated emotions. *Nat. Neurosci.* 3, 1049–1056.
- Damoiseaux, J.S., Rombouts, S.A., Barkhof, F., Scheltens, P., Stam, C.J., Smith, S.M., Beckmann, C.F., 2006. Consistent resting-state networks across healthy subjects. *Proc. Natl. Acad. Sci. U. S. A.* 103, 13848–13853.
- Deco, G., Jirsa, V.K., McIntosh, A.R., 2011. Emerging concepts for the dynamical organization of resting-state activity in the brain. *Nature reviews. Neuroscience* 12, 43–56.
- Deen, B., Pitskel, N.B., Pelphrey, K.A., 2011. Three systems of insular functional connectivity identified with cluster analysis. *Cereb. Cortex* 21, 1498–1506.
- Di Martino, A., Shehzad, Z., Kelly, C., Roy, A.K., Gee, D.G., Uddin, L.Q., Gotimer, K., Klein, D.F., Castellanos, F.X., Milham, M.P., 2009. Relationship between cingulo-insular functional connectivity and autistic traits in neurotypical adults. *Am. J. Psychiatry* 166, 891–899.
- Dodds, C.M., Morein-Zamir, S., Robbins, T.W., 2011. Dissociating inhibition, attention, and response control in the frontoparietal network using functional magnetic resonance imaging. *Cereb. Cortex* 21, 1155–1165.
- Dosenbach, N.U., Visscher, K.M., Palmer, E.D., Miezin, F.M., Wenger, K.K., Kang, H.C., Burgund, E.D., Grimes, A.L., Schlaggar, B.L., Petersen, S.E., 2006. A core system for the implementation of task sets. *Neuron* 50, 799–812.
- Dosenbach, N.U., Fair, D.A., Miezin, F.M., Cohen, A.L., Wenger, K.K., Dosenbach, R.A., Fox, M.D., Snyder, A.Z., Vincent, J.L., Raichle, M.E., Schlaggar, B.L., Petersen, S.E., 2007. Distinct brain networks for adaptive and stable task control in humans. *Proc. Natl. Acad. Sci. U. S. A.* 104, 11073–11078.
- Dosenbach, N.U., Fair, D.A., Cohen, A.L., Schlaggar, B.L., Petersen, S.E., 2008. A dual-networks architecture of top-down control. *Trends Cogn. Sci.* 12, 99–105.
- Downar, J., Crawley, A.P., Mikulis, D.J., Davis, K.D., 2002. A cortical network sensitive to stimulus salience in a neutral behavioral context across multiple sensory modalities. *J. Neurophysiol.* 87, 615–620.
- Eckert, M.A., Menon, V., Walczak, A., Ahlstrom, J., Denslow, S., Horwitz, A., Dubno, J.R., 2009. At the heart of the ventral attention system: the right anterior insula. *Hum. Brain Mapp.* 30, 2530–2541.
- Eichele, T., Debener, S., Calhoun, V.D., Specht, K., Engel, A.K., Hugdahl, K., von Cramon, D.Y., Ullsperger, M., 2008. Prediction of human errors by maladaptive changes in event-related brain networks. *Proc. Natl. Acad. Sci. U. S. A.* 105, 6173–6178.
- Fox, M.D., Raichle, M.E., 2007. Spontaneous fluctuations in brain activity observed with functional magnetic resonance imaging. *Nature reviews. Neuroscience* 8, 700–711.
- Fox, M.D., Snyder, A.Z., Vincent, J.L., Raichle, M.E., 2007. Intrinsic fluctuations within cortical systems account for intertrial variability in human behavior. *Neuron* 56, 171–184.
- Goldman-Rakic, P.S., 1988. Topography of cognition: parallel distributed networks in primate association cortex. *Annu. Rev. Neurosci.* 11, 137–156.
- Gu, X., Liu, X., Guise, K.G., Naidich, T.P., Hof, P.R., Fan, J., 2010. Functional dissociation of the fronto-insular and anterior cingulate cortices in empathy for pain. *J. Neurosci.* 30, 3739–3744.
- Hampson, M., Driesen, N.R., Skudlarski, P., Gore, J.C., Constable, R.T., 2006. Brain connectivity related to working memory performance. *J. Neurosci.* 26, 13338–13343.
- Heining, M., Young, A.W., Ioannou, G., Andrew, C.M., Brammer, M.J., Gray, J.A., Phillips, M.L., 2003. Disgusting smells activate human anterior insula and ventral striatum. *Ann. N. Y. Acad. Sci.* 1000, 380–384.
- Hua, H., Strigo, I.A., Baxter, L.C., Johnson, S.C., Craig, A.D., 2005. Anteroposterior somatotopy of innocuous cooling activation focus in human dorsal posterior insular cortex. *Am. J. Physiol. Regul. Integr. Comp. Physiol.* 289, R319–R325.
- Jabbi, M., Bastiaansen, J., Keysers, C., 2008. A common anterior insula representation of disgust observation, experience and imagination shows divergent functional connectivity pathways. *PLoS One* 3, e2939.
- Kaller, C.P., Rahm, B., Spreer, J., Weiller, C., Unterrainer, J.M., 2011. Dissociable contributions of left and right dorsolateral prefrontal cortex in planning. *Cereb. Cortex* 21, 307–317.
- Kober, H., Barrett, L.F., Joseph, J., Bliss-Moreau, E., Lindquist, K., Wager, T.D., 2008. Functional grouping and cortical-subcortical interactions in emotion: a meta-analysis of neuroimaging studies. *NeuroImage* 42, 998–1031.
- Kurth, F., Zilles, K., Fox, P.T., Laird, A.R., Eickhoff, S.B., 2010. A link between the systems: functional differentiation and integration within the human insula revealed by meta-analysis. *Brain Struct. Funct.* 214, 519–534.
- LaBar, K.S., Gitelman, D.R., Parrish, T.B., Kim, Y.H., Nobre, A.C., Mesulam, M.M., 2001. Hunger selectively modulates corticostriatal activation to food stimuli in humans. *Behav. Neurosci.* 115, 493–500.
- Lang, P.J., Bradley, M.M., Cuthbert, B.N., 1997. International Affective Picture System (IAPS): Technical Manual and Affective Ratings. NIMH Center for the Study of Emotion and Attention, Gainesville, FL.
- Lewis, C.M., Baldassarre, A., Committeri, G., Romani, G.L., Corbetta, M., 2009. Learning sculpt the spontaneous activity of the resting human brain. *Proc. Natl. Acad. Sci. U. S. A.* 106, 17558–17563.
- Lindquist, K.A., Wager, T.D., Kober, H., Bliss-Moreau, E., LF, B., in press. The brain basis of emotion: A meta-analytic review. *Behavioral & Brain Sciences* 35.
- Mason, M.F., Norton, M.I., Van Horn, J.D., Wegner, D.M., Grafton, S.T., Macrae, C.N., 2007. Wandering minds: the default network and stimulus-independent thought. *Science* 315, 393–395.
- Menon, V., Uddin, L.Q., 2010. Salience, switching, attention and control: a network model of insula function. *Brain Struct. Funct.* 214, 655–667.
- Mesulam, M.M., 1998. From sensation to cognition. *Brain* 121 (Pt 6), 1013–1052.
- Mesulam, M.M., Mufson, E.J., 1982a. Insula of the old world monkey. I. Architectonics in the insulo-orbito-temporal component of the paralimbic brain. *J. Comp. Neurol.* 212, 1–22.
- Mesulam, M.M., Mufson, E.J., 1982b. Insula of the old world monkey. III: Efferent cortical output and comments on function. *J. Comp. Neurol.* 212, 38–52.
- Moriguchi, Y., Negreira, A., Weierich, M., Dautoff, R., Dickerson, B.C., Wright, C.I., Barrett, L.F., 2011. Differential hemodynamic response in affective circuitry with aging: an fMRI study of novelty, valence, and arousal. *J. Cogn. Neurosci.* 23, 1027–1041.
- Mufson, E.J., Mesulam, M.M., 1982. Insula of the old world monkey. II: Afferent cortical input and comments on the claustrum. *J. Comp. Neurol.* 212, 23–37.
- Mutschler, I., Wieckhorst, B., Kowalevski, S., Derix, J., Wentlandt, J., Schulze-Bonhage, A., Ball, T., 2009. Functional organization of the human anterior insular cortex. *Neurosci. Lett.* 457, 66–70.
- Nagai, Y., Critchley, H.D., Featherstone, E., Trimble, M.R., Dolan, R.J., 2004. Activity in ventromedial prefrontal cortex covaries with sympathetic skin conductance level: a physiological account of a “default mode” of brain function. *NeuroImage* 22, 243–251.
- Nelson, S.M., Dosenbach, N.U., Cohen, A.L., Wheeler, M.E., Schlaggar, B.L., Petersen, S.E., 2010. Role of the anterior insula in task-level control and focal attention. *Brain Struct. Funct.* 214, 669–680.
- Phan, K.L., Taylor, S.F., Welsh, R.C., Ho, S.H., Britton, J.C., Liberzon, I., 2004. Neural correlates of individual ratings of emotional salience: a trial-related fMRI study. *NeuroImage* 21, 768–780.
- Reitan, R.M., 1958. Validity of the Trail Making Test as an indication of organic brain damage. *Percept. Mot. Ski.* 8, 271–276.
- Sadaghiani, S., Scheeringa, R., Lehongre, K., Morillon, B., Giraud, A.L., Kleinschmidt, A., 2010. Intrinsic connectivity networks, alpha oscillations, and tonic alertness: a simultaneous electroencephalography/functional magnetic resonance imaging study. *J. Neurosci.* 30, 10243–10250.
- Schulz, K.P., Bedard, A.C., Czamecki, R., Fan, J., 2011. Preparatory activity and connectivity in dorsal anterior cingulate cortex for cognitive control. *NeuroImage* 57, 242–250.
- Seeley, W.W., Menon, V., Schatzberg, A.F., Keller, J., Glover, G.H., Kenna, H., Reiss, A.L., Greicius, M.D., 2007. Dissociable intrinsic connectivity networks for salience processing and executive control. *J. Neurosci.* 27, 2349–2356.
- Shulman, G.L., Astafiev, S.V., Franke, D., Pope, D.L., Snyder, A.Z., McAvoy, M.P., Corbetta, M., 2009. Interaction of stimulus-driven reorienting and expectation in ventral and dorsal frontoparietal and basal ganglia-cortical networks. *J. Neurosci.* 29, 4392–4407.
- Small, D.M., 2010. Taste representation in the human insula. *Brain Struct. Funct.* 214, 551–561.
- Small, D.M., Zatorre, R.J., Dagher, A., Evans, A.C., Jones-Gotman, M., 2001. Changes in brain activity related to eating chocolate: from pleasure to aversion. *Brain* 124, 1720–1733.
- Spreng, R.N., Stevens, W.D., Chamberlain, J.P., Gilmore, A.W., Schacter, D.L., 2010. Default network activity, coupled with the frontoparietal control network, supports goal-directed cognition. *NeuroImage* 53, 303–317.
- Sridharan, D., Levitin, D.J., Menon, V., 2008. A critical role for the right fronto-insular cortex in switching between central-executive and default-mode networks. *Proc. Natl. Acad. Sci. U. S. A.* 105, 12569–12574.
- Stevens, W.D., Buckner, R.L., Schacter, D.L., 2010. Correlated low-frequency BOLD fluctuations in the resting human brain are modulated by recent experience in category-preferential visual regions. *Cereb. Cortex* 20, 1997–2006.
- Strauss, E., Sherman, E.M.S., Spreen, O., 2006. A compendium of neuropsychological tests: administration, norms, and commentary, 3rd ed. Oxford University Press, Oxford; New York.
- Tambini, A., Keiz, N., Davachi, L., 2010. Enhanced brain correlations during rest are related to memory for recent experiences. *Neuron* 65, 280–290.
- Taylor, K.S., Seminowicz, D.A., Davis, K.D., 2009. Two systems of resting state connectivity between the insula and cingulate cortex. *Hum. Brain Mapp.* 30, 2731–2745.
- Van Dijk, K.R., Hedden, T., Venkataraman, A., Evans, K.C., Lazar, S.W., Buckner, R.L., 2010. Intrinsic functional connectivity as a tool for human connectomics: theory, properties, and optimization. *J. Neurophysiol.* 103, 297–321.
- Vincent, J.L., Patel, G.H., Fox, M.D., Snyder, A.Z., Baker, J.T., Van Essen, D.C., Zempel, J.M., Snyder, L.H., Corbetta, M., Raichle, M.E., 2007. Intrinsic functional architecture in the anaesthetized monkey brain. *Nature* 447, 83–86.
- Vincent, J.L., Kahn, I., Snyder, A.Z., Raichle, M.E., Buckner, R.L., 2008. Evidence for a frontoparietal control system revealed by intrinsic functional connectivity. *J. Neurophysiol.* 100, 3328–3342.
- Wager, T.D., Barrett, L.F., 2004. From affect to control: Functional specialization of the insula in motivation and regulation. Published online at *PsyExtra*.
- Wager, T., Barrett, L., Bliss-Moreau, E., Lindquist, K., Duncan, S., Kober, H., Joseph, J., Davidson, M., Mize, J., 2008. The neuroimaging of emotion. In: Lewis, M., Haviland-Jones, J., Barrett, L. (Eds.), *The handbook of emotion*. Guilford, New York, pp. 249–271.
- Wang, L., Laviolette, P., O’Keefe, K., Putcha, D., Bakkour, A., Van Dijk, K.R., Pihlajamaki, M., Dickerson, B.C., Sperling, R.A., 2010a. Intrinsic connectivity between the hippocampus and posteromedial cortex predicts memory performance in cognitively intact older individuals. *NeuroImage* 51, 910–917.
- Wang, L., Negreira, A., Laviolette, P., Bakkour, A., Sperling, R.A., Dickerson, B.C., 2010b. Intrinsic interhemispheric hippocampal functional connectivity predicts individual differences in memory performance ability. *Hippocampus* 20, 345–351.
- Weierich, M.R., Wright, C.I., Negreira, A., Dickerson, B.C., Barrett, L.F., 2010. Novelty as a dimension in the affective brain. *NeuroImage* 49, 2871–2878.
- Weissman, D.H., Roberts, K.C., Visscher, K.M., Woldorff, M.G., 2006. The neural bases of momentary lapses in attention. *Nat. Neurosci.* 9, 971–978.
- Yeo, B.T., Krienen, F.M., Sepulcre, J., Sabuncu, M.R., Lashkari, D., Hollinshead, M., Roffman, J.L., Smoller, J.W., Zolke, L., Polimeni, J.R., Fischl, B., Liu, H., Buckner, R.L., 2011. The organization of the human cerebral cortex estimated by intrinsic functional connectivity. *J. Neurophysiol.* 106, 1125–1165.